Hybrid epoxy-SiO$_2$/GO nanosheets anti-corrosive coating for aeronautic aluminum Al6061-T5

Jevet E. D. López-Campos, José Mojica-Gómez, Alfredo Maciel-Cerda, Víctor M. Castaño, Genoveva Hernández-Padrón

Abstract The mechanical and anti-corrosive evaluation of a hybrid epoxy resin–SiO$_2$ and graphene oxide (GO) are presented. Three composite materials were prepared with 0%, 0.1 wt% and 0.5 wt% GO concentrations. The hybrid material was prepared by the sol-gel process incorporating the silica particles in situ within the epoxy resin (ER) matrix and previously that ER was functionalized with carboxyl groups using abietic acid and labeled as functionalized epoxy resin. The deposition of the three hybrids in aluminum 6061 substrates was made by blade coating, measuring wet and dry film thickness. The study of mechanical properties involved adhesion, pencil scratch hardness, and abrasion test methods where the incorporation of 0.5 wt% of GO improved the mechanical properties considerably. The anti-corrosive properties of the coatings were evaluated through electrochemical impedance spectroscopy and accelerated corrosion using a salt spray chamber showing that GO forms an anti-corrosive barrier increasing the operation life of the coatings in corrosive environments. Anti-ice properties were related to the contact angle measurement from which the GO concentrations showed more hydrophobic behavior. All the tests were carried out according to ASTM standards. The incorporation of 0.5% of GO showed a significant improvement in the mechanical and anti-corrosive results, improving corrosion resistance up to 500 h. The abrasion tests had an increase in 35%, its hardness up to 9H, and the wear index improved by 29.14% compared with composites with 0.1 wt% of GO and without GO. The HREF1 and HREF5 materials do present an increase in the contact angle thanks to the incorporation of graphene oxide. The results of electrochemical impedance spectroscopy and the impedance curves show a better behavior for the HREF5 composite due to the difference in resistance over time.

Keywords Hybrid epoxy resin, GO nanosheets, Aeronautic, Anti-corrosion coating

J. E. D. López-Campos
Centro de Física Aplicada y Tecnología Avanzada, PCeIM, UNAM, Juriquilla, Querétaro, Mexico
e-mail: jevet.lopez@gmail.com

J. Mojica-Gómez
Centro de Investigación y Desarrollo Tecnológico en Electroquímica, Parque San Fandila S/N, Pedro Escobedo, Querétaro, Mexico
e-mail: jmojica@cideteq.mx

A. Maciel-Cerda
Instituto de Investigaciones en Materiales, Ciudad Universitaria, UNAM, Mexico City, Mexico
e-mail: macielal@unam.mx

V. M. Castaño
Centro de Física Aplicada y Tecnología Avanzada, Departamento de Ciencia e Ingeniería de Materiales, UNAM, Juriquilla, Querétaro, Mexico
e-mail: vmcastano@unam.mx

G. Hernández-Padrón (✉)
Centro de Física Aplicada y Tecnología Avanzada, Departamento de Nanotecnología, UNAM, Juriquilla, Querétaro, Mexico
e-mail: genoveva@unam.mx

Introduction

Degradation can be defined as the deterioration of a material due to the action of the environment in which it is immersed (pressure, humidity, mechanical stress, pH of fluids, atmospheric chemical agents, etc.) causing the loss of physical and mechanical properties of the material. When speaking of corrosion, it is understood only as the chemical or electrochemical degradation of a material, usually a metal, by its environment.[1,2]

Organic coatings including epoxy primers have become a common solution to protect metal substrates against corrosion and environmental erosion, leading to a great development in the materials used to improve the properties of the coatings.[3] Due to the outstanding features of this type of coating, nanofillers are being introduced to produce hybrid materials, combining organic and inorganic properties and enhancing the protective applications.[4] For instance, Araki et al.[5] have studied the effect of the viscoelasticity of epoxy/silica hybrids in terms of morphology. Also, silica has been used in polyimides[6] and poly(tetramethylene oxide)[7] organic coatings to study the resistance against the attack of atomic oxygen. Wang et al.[8] tested tubes of a nano-silica/graphene oxide hybrid to study the flame retarding effect and thermal conductivity. Silica is not the only inorganic nanofiller. Zhao et al.[9] modified the surface of ZrO_2 nanoparticles with a styrene coupling agent and used them as an additive to improve corrosion protection. Most authors conclude that nanofillers help organic coatings because the microporosity diminishes blocking the way for corrosion.

Hybrid coatings also represent a promising solution in the aerospace industry to stop using anti-corrosive protective systems based on electrochemical salt baths to form chromates.[2] Hexavalent chromium has good corrosion resistance due to its strong rust-preventing properties. However, it is a great enemy to the environment and highly toxic for humans.[10] Furthermore, there are extensive investigations into the diversity of nanofillers for hybrid materials applied in the aeronautical sector to provide more benefits besides corrosion protection such as anti-icing/de-icing properties.[11–14]

Multiple works can be found where the improvement of clear epoxy resin with SiO_2 nanoparticles or nanoclusters is analyzed in many mechanical, chemical, or thermal aspects[15] and by different synthesis routes.[16] Thus, the improvement of clear resin by adding silica nanoparticles is already a known fact and we elaborate in this paper on more technical details about the structure and the interesting and novel improvement on corrosion resistance.

Graphene oxide (GO) is of interest to this work because of its impermeability against diffusion of water, oxygen, and corrosive Cl⁻ ions; therefore, it acts as a barrier in the coatings.[17] Recently, Parhizkar et al.[18] and Pourhashem et al.[19] have studied the corrosion protection of epoxy coatings on steel substrates enhancing the interfacial adhesion with modified amino-functionalized GO. In addition, GO research also affects the thermal performance and stability.[20] Ramezanzadeh's group has investigated the interaction between silica particles and GO sheets through different publications, and recently covered the coating systems.[21–23] Nevertheless, there is no reported information on using a functionalized epoxy matrix or electrochemical results for aeronautical aluminum as the coated substrate.

Thus, the objective of this work was to study the effect of GO on the mechanical and anti-corrosive properties within a functionalized epoxy-SiO_2 hybrid, characterizing the material with different techniques and test methods to evaluate the properties as a coating material for aluminum 6061-T5.

Materials

Natural mineral graphite powder (90%) was generously donated by Mr. Alfredo Ayala, of the Centro de Física Aplicada y Tecnología Avanzada (CFATA). Chemical reagents for the synthesis of graphene oxide (GO), sulfuric acid (H_2SO_4, 98 wt%), hydrogen peroxide (H_2O_2, 30%), hydrochloric acid (HCl), and potassium permanganate ($KMnO_4$, 99.5 wt%) were acquired from Sigma-Aldrich. Tetraethyl orthosilicate (TEOS, 98 wt%), ethanol (C_2H_5OH, 98 wt%), and sodium hydroxide (NaOH, 98%) were purchased from Sigma-Aldrich. Abietic acid ($C_{20}H_{30}O_2$, 97%) was obtained from Sigma-Aldrich, and bisphenol/epichlorohydrin epoxy resin with Mn = 700 was bought from Poliformas plásticas. The curing agent used to prepare the coatings was polyoxypropylendiamine "HD-307" with a specific gravity of 0.97 ± 0.02 and viscosity of 3500 mPa.s at 25°C and was from Poliformas plásticas. Materials for the ASTM test methods included a set of standard pencils, weighted standard car for hardness, adhesion tape, and a 1-mm/2-mm metallic grid.

Methodology

Synthesis

Graphite oxide (GrO) was synthesized from natural mineral graphite by the modified Hummers method.[24] This process consisted of dispersing 2 g of graphite powder in 46 mL of H_2SO_4 at -5°C in an ice bath immersed flask under constant stirring; then, 6 g of $KMnO_4$ was gradually added keeping the temperature below 20°C. Once homogenized, the mixture was removed from the ice bath, brought up to 35°C to initiate the reaction and maintained for 2 h. Then, 92 mL of distilled water was added drop-by-drop, maintaining the stirring for 15 min. The reaction was terminated by transferring the mixture to a vessel with 270 mL of distilled water and 10 mL of H_2O_2 (30% v/v). Subsequently, centrifugation washes were performed using 400 mL of an HCl solution (2.5% v/v) to remove metal ions and distilled water until obtaining a pH close to 7. Finally, the graphene oxide was obtained from the exfoliation of the stacked sheets in the graphite oxide, through the dispersion of batches of 300 mg of GrO in distilled water (10 mg/mL) and subjected to an ultrasonic bath treatment (42 kHz $\pm$

6%) for 3 h. The product was then dried to obtain a black GO powder.

On the other hand, 40 g of epoxy resin (Mn = 700) and 0.85 g (0.003 mol) of abietic acid were mixed with stirring for 20 min at a temperature between 95°C and 115°C to obtain functionalized epoxy resin (FER).

The hydrolysis sol-gel[25] process was made with a TEOS: EtOH solution (13.75:5 v/v) mixed with a previous 30-min ultrasonic bathed water: EtOH:GO solution (5:20:x v/v/m) with constant stirring and at a temperature of 95°C, where x represents 0 g (0 wt%), 0.04 g (0.1 wt%), and 0.2 g (0.5 wt%) of GO powder for the three hybrids. After 30 min, 40 g of FER were added dropwise and the mixture was left under reflux for 1 h at 105°C, and the viscosity was monitored visually.

Preparation of aluminum substrates

For the adhesion and hardness mechanical characterization of the coating-substrate system, nine 8×8 cm^2 aluminum samples were machined, and sanded with a ¼'' orbital sander up to 360 sandpaper. For the abrasion test, nine 10×10 cm^2 samples with rounded corners ($r = 1$ cm) and a central hole of $D = 1/2$'' aluminum specimens were machined, sanded with a ¼'' orbital sander up to 360 sandpaper. All samples were cleaned in a 15-min isopropanol ultrasonic bath and 15-min acetone ultrasonic bath.

Preparation of hybrid coatings

To study the mechanical properties as a coating, the hybrid epoxy coatings containing 0% (HREF), 0.1% GO (HREF1), and 0.5% GO (HREF5) were prepared with the polyamine curing method for epoxy polymers. The prepared solutions were mixed with the polyoxypropylendiamine HD-307 commercial hardener in a ratio of 100:15 m/m, followed by a 5-min ultrasonic bath to eliminate any air bubbles trapped. Then, the resin was kept for 10 min in a chamber at 30°C to evaporate any solvent remanent to evaporate due to the curing exothermic reaction. Finally, the hybrid coatings were carefully blade coated on the cleansed aluminum substrates and dried at room temperature for 5 h for the first dry, and then a second dry for 24 h for a total drying.[26] The wet thickness of the coatings (about 45 ± 10 μm) was established with the two micrometers in the blade-coating equipment.

Characterization

X-ray diffraction (XRD) analysis was used to verify the oxidation of mineral graphite and the exfoliation to obtain GO sheets. The equipment was a Rigaku Ultima IV diffractometer, equipped with an X-ray generator with a maximum power of 3 kW, voltage of 20–60 kV, and output current of 2–60 mA from 5° to 80°.

Raman dispersive spectra were carried out to confirm graphene oxide using a Bruker model Senterra with an optic microscope 20× objective, with a resolution of 9–15 cm^{-1}, an integration time of 2 s, 8 scans, and power of 25 mW. The spectra were recorded in the 110–3400 cm^{-1}.

Attenuated total reflectance–Fourier transformed infrared (ATR-FTIR) spectra measurements were achieved using a Thermo Scientific Model Nicolet 6700, with a scan speed of 0.32 s, a gain of 8.00, and a voltage (Vpp) of 5.73 V. The spectra were recorded in the wavenumber range between 4000 cm^{-1} and 400 cm^{-1} at a resolution of 4 cm^{-1}.

Scanning electron microscopy (SEM) was used to observe the dispersion quality and the morphology of the hybrids, the equipment was a SU8230 Hitachi SEM/STEM CFE, and the samples were gold coated using an AMS Au-Coater. The sample for transmission electron microscopy (TEM) was prepared by dispersing GO in distilled water and placed and dried in the TEM grid. Afterward, it was observed with 60–80 kV in a JEOL TEM 1010 microscope.

To be considered in the aeronautical market, the *ASTM D-2369-20 Standard Test Method for Volatile Content of Coatings*[27] was conducted.

Mechanical tests

The adhesion strength, hardness, and abrasion of the different hybrid material samples were studied by the ASTM Standard Methods:

- *ASTM D3363-20 Standard Test Method for Film Hardness by Pencil Test*

A coated panel is placed on a firm horizontal surface. The pencil is held firmly, with a calibrated 1 kg-weighed trolley, against the film at a 45° angle (point away from the operator) and pushed away from the operator in a 6.5-mm (1/4 in.) stroke. The process is started with the hardest pencil (9H) and continued down the scale of hardness to either of two endpoints: one, the pencil that will not cut into or gouge the film (pencil hardness), or two, the pencil that will not scratch the film (scratch hardness), with 9B being the softest pencil.[28]

- *ASTM D4060-19; Standard Test Method for Abrasion Resistance of Organic Coatings by Taber Abraser*

The organic coating is applied at a uniform thickness to a plane, rigid panel. After curing, the surface is abraded by rotating the panel under weighted abrasive wheels. Abrasion resistance is calculated as loss in

weight at a specified number of abrasion cycles, as loss in weight per cycle, or as a maximum number of cycles required to remove all the coating thickness in at least one spot.[29]

- *ASTM D3359-17 Standard Test Methods for Rating Adhesion by Tape Test*

Test Method B—A lattice pattern with either six (0–50 μm coating thickness) or eleven (50–100 μm coating thickness) cuts in each direction is made through the film to the substrate, and the pressure-sensitive tape is applied over the lattice pattern and then removed. The adhesion rate is assessed qualitatively on a 0 to 5 scale.[30] Previous to the test according to the ASTM D3359 method, the coating thickness where the test is performed was measured using an Elcometer 456 instrument.

Corrosion test

The corrosion resistance, the electrochemical behavior, and hydrophobicity of HREF, HREF1, and HREF5 were tested under the *ASTM B117-19 Standard Practice for Salt Spray (Fog) Apparatus*, saline immersion with artificial defect, electrochemical impedance spectroscopy (EIS) and contact angle. The salt fog test was carried out in a Q-FOG Cyclic Corrosion Tester 1100 with a 5%-NaCl (99%) solution using distilled water type 4 with 6.5−7.2 pH and specific gravity of 0.85−0.92, at 35°C, and > 95% humidity. The time measured for the first sign of corrosion to appear on the substrate was evaluated, and the number of hours for this first sign to appear for each applied coating is recorded. *Standard ISO-4628, Paints and Varnishes—Evaluation of Degradation of Coatings,* was applied to classify the quantity, size, and intensity of uniform changes in appearance/defects after they have been subjected for a certain time to the accelerated corrosion test.

Saline immersion was performed in a 5%-NaCl solution for 500 h under normal conditions, and artificial defects, simulating a 2-mm grid, were made in the coated substrates to be analyzed.

The EIS test was carried out in a classic three-electrode cell, shown in Fig. 1, consisting of a saturated solution of KCl in an Ag/AgCl reference electrode, graphite as the counter-electrode, and aluminum substrates coated as the working electrode, the exposure area was 15.2 cm^2. The open circuit potential (OCP) is first established to start the measurements in 5 wt% NaCl aqueous solution at different immersion times of 0, 170, and 340 h. The alternating current (AC) impedance was carried out at the OCP with an amplitude of ± 10 mV in the frequency range between 100 KHz and 10 mHz using a Bio-Logic VMP3 potentiostat. The obtained curves were analyzed with the EC-Lab V11.41 software.
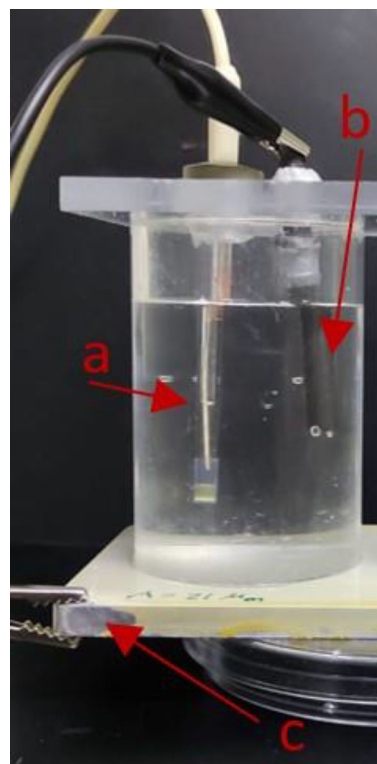

Fig. 1: Electrochemical cell. (a) Ag/AgCl reference electrode, (b) graphite counter-electrode and (c) working electrode

To measure the hydrophobicity, a contact angle test was performed on eight points of the coated substrates analyzing the digital photography with ImageJ software. All tests were repeated three times for reproducibility.

Results and discussion

GO nanosheets characterization

To confirm the graphene oxide synthesis, techniques such as X-ray diffraction (XRD) and dispersive Raman spectroscopy are performed. For mineral graphite, we can observe in Fig. 2a the characteristic peak of graphite at $2\theta = 26.4°$ (002) and the peaks with less intensity (110) and (222) are also attributed to graphite with hexagonal structure.[31] Figure 2b shows the XRD after the modified Hummers method for GO with the presence of the peak at $2\theta = 13.86°$ (d-spacing 6.4865 Å) characteristic of graphene oxide (GO), and the peaks that appear at $2\theta = 26.5°$ and $2\theta = 43.1°$ indicate that there is still a presence of mineral graphite in the sample.

Figure 2c shows the Raman spectrum indicating the clear difference of intensities and band width between graphite oxide (GrO-P) and graphene oxide (GO-P). Also, characteristic bands of the GrO and GO are
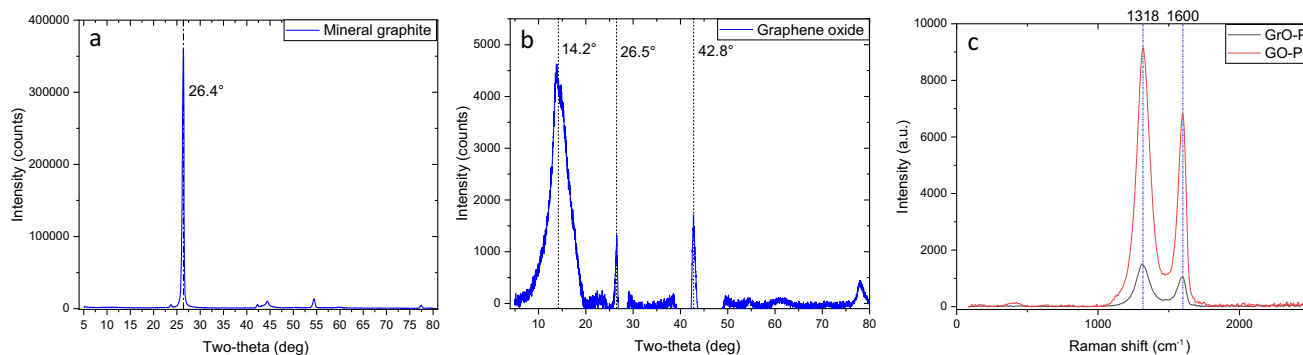
Fig. 2: (a) XRD for mineral graphite; (b) XRD for GO and (c) Raman spectra for graphene oxide (GO-P) and graphite oxide (GrO-P)

present for D band at 1335 and 1350 cm^{-1} and G band at 1595 and 1597 cm^{-1}, where it is possible to observe more intensity and smaller width for GO.[32]

Spectroscopic coatings characterization

Different FTIR spectra for the HREF, HREF1, and HREF5 samples are shown in Fig. 3. In the HREF spectrum, it is possible to observe the signal in the absorption band at 1727 cm^{-1}, this signal corresponds to the carboxyl group of abietic acid. The absorption band at 1237 cm^{-1} is related to the C–O bend, and the bands from 800 cm^{-1} to 824 cm^{-1} are originated by the C–H groups. Bands corresponding to Si–O–Si symmetric and asymmetric vibrations are located at 874 cm^{-1} and 1084 cm^{-1}, respectively.[33] In previous works,[26,33] we have described in detail the chemical structure of epoxy resin and functionalized epoxy resin by FTIR and Raman spectroscopy.

The absorption bands at 750 cm^{-1} and 560 cm^{-1} correspond to the C–O bonds, and the bands at 2918 cm^{-1} and 2850 cm^{-1} are due to the CH$_2$ asymmetric and symmetric stretching, respectively. Finally, the absorption band at 2960 cm^{-1} indicates the presence of CH$_3$ symmetric groups.

As for the functionalized epoxy resin (REF) with 1 y 5% GO, HREF1 and HREF5, respectively, the depicted FTIR bands are, in principle, similar to those of REF, with some important shifts at 1084 cm^{-1} and 874 cm^{-1} bands, which indicate the interaction between graphene oxide and the SiO$_2$ particles. It is suggested that the intensity and width of those bands increased because of the better distribution due to the silica presence around the GO sheets.

Figure 4 corresponds to Raman spectra of HREF, HREF1, and HFE5 hybrid samples, showing epoxy characteristic bands due to C=C double bonds at 1607 cm^{-1}. Between the range of 1230 cm^{-1} and 1280 cm^{-1}, the bands correspond to the vibration of the epoxy group, and the intensity of this range of bands is linearly dependent on the concentration of epoxy groups present in the resin. The band at
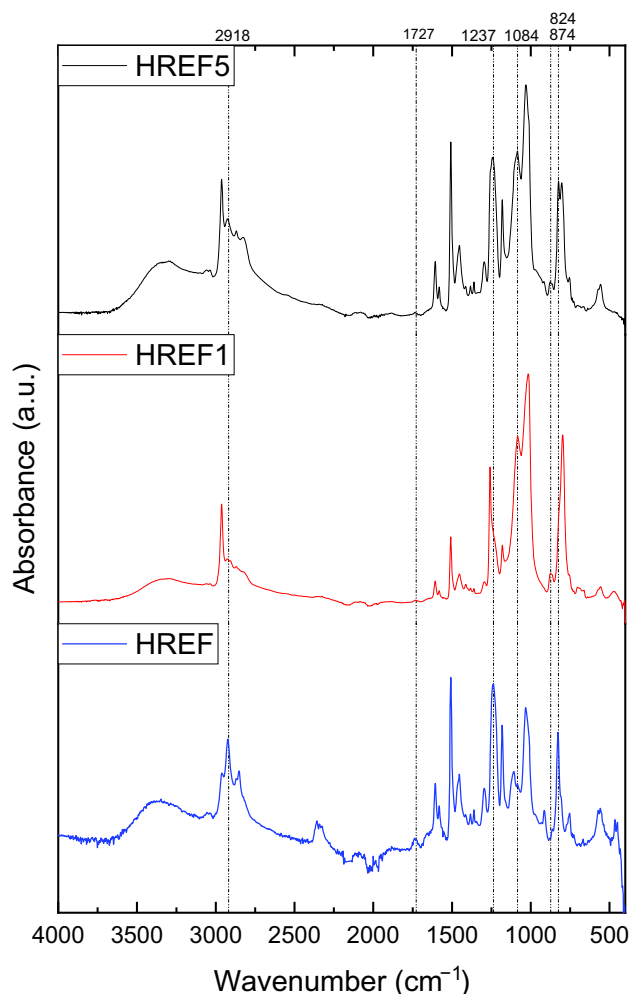

Fig. 3: FTIR spectra of HREF5 (black), HREF1 (red), and HREF (without GO, blue)

916 cm^{-1} is assigned to the deformation of the epoxy rings, being less intense. The bands at 643 cm^{-1} and 1458 cm^{-1} identify the aromatic rings. The bands above 2800 cm^{-1} correspond to the CH$_3$ and CH$_2$ groups. The Raman spectroscopy for REF does not
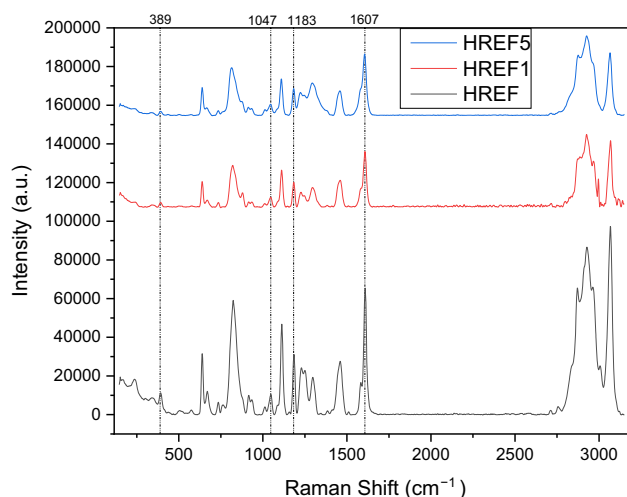
Fig. 4: Raman spectra of HREF (without GO, black), HREF1 (red), and HREF5 (blue) (Color figure online)

provide any clear or concrete indication about the functionalization, due to the concentration of abietic acid used.[33]

The Raman spectra for the HREF1 and HREF5 samples show bands located at 1183 cm^{-1} caused by the Si–O–Si bond. The bands at 1047 cm^{-1} are assigned to Si–O bonds. The band found at 389 cm^{-1} corresponds to the formation of the SiO$_2$ network.[5] The intensity of the signal that appears at 1607 cm^{-1} decreases, and a band broadening is also found, that is a function of the increase in GO concentration, indicating an interaction between the resin and the SiO$_2$/GO in the hybrid materials. This behavior of the spectra of the materials with graphene oxide at different concentrations, HREF1 and HREF5, indicates that there is graphene oxide decorated with silica particles and present in an epoxy medium.

SEM characterization

A micrograph for HREF is shown in Fig. 5a, where the SiO$_2$ particles can be observed individually with a diameter of approximately 80 nm embedded in the epoxy resin forming also bigger agglomerations around 2 μm, this with an x20.0 k objective. Figure 5b shows a better dispersion of the SiO$_2$ particles embedded in the HREF1 resin matrix and fewer agglomerations within the material and with a mean size distribution of 60 nm and a resolution of 20.0 k. Figure 5c shows HREF1 micrograph, where it is possible to observe the hybrid materials containing a structure of GO nanosheets surfaces decorated with smaller silica particles around 24–34 nm in size. For the HREF5 hybrid, Fig. 5d, e, in this case, can observe the best homogeneity, compared with HRREF and HREF1, with fewer aggregates of 40–50 nm particles with an amplification of x150.0 k. In general, we can say that the particles are well dispersed in the material.

Figure 5f shows a micrograph by transmission electron microscopy for graphene oxide, which shows that the material does have a laminated structure, both the degree of oxidation and the laminated structure are responsible for the links between the graphene oxide graphene and REF/SiO$_2$ particles. Also, the presence of graphene oxide and the SiO$_2$ particles will have an impact on the interaction with the ion flux, due to the impermeability of the graphene oxide sheets and their decoration with SiO$_2$ particles.

Mechanical characterization

The adhesion rate, pencil scratch hardness, and abrasion results for the three hybrid materials are shown in Table 1, where the thickness is specified for the area where the test was performed.

Figure 6a–c shows the resulting surfaces of the substrates after conducting the adhesion test for HREF, HREF1, and HREF5, respectively. Figure 6a–c shows 45%, 5%, and 0% of removed coating, respectively. The classification was given accordingly to the percent area removed specified in the ASTM standard. Figure 4d exposes the criteria to end the Taber abrasion testing when the first sight of the metallic substrate is revealed.

In addition, the abrasion test can measure the wear index following the calculations as specified in the *ASTM D4060-19*:

$$I = \frac{(A - B)1000}{C}$$

Where I = wear index, A = original weight, B = weight after "C" cycles of abrasion, C = cycles of abrasion

The outcome of the calculations is shown in Table 2 for the hybrid materials. With a lower wear index, the greater the abrasion resistance the coating has.

Accelerated corrosion

Aluminum plates coated with the three hybrid coatings were evaluated for 500 h in a salt fog spray chamber, making observations approximately every 168 h (7 days). The qualitative analysis is reported as follows with a magnifying glass:

Figure 7a shows the HREF sample in the initial state, and the analysis at different experimental times. At 170 h, Fig. 7b, no defects were found. After 340 h, Fig. 7c shows the start of three defects. In both lower corners, corrosion has penetrated the coating generating moisture in between the substrate and the coating (Classification 3S4(4) and 3S3(3)), in Fig. 7d pointed in the middle section of the plate, a major blister is affecting the coated specimen (3S5(4)).
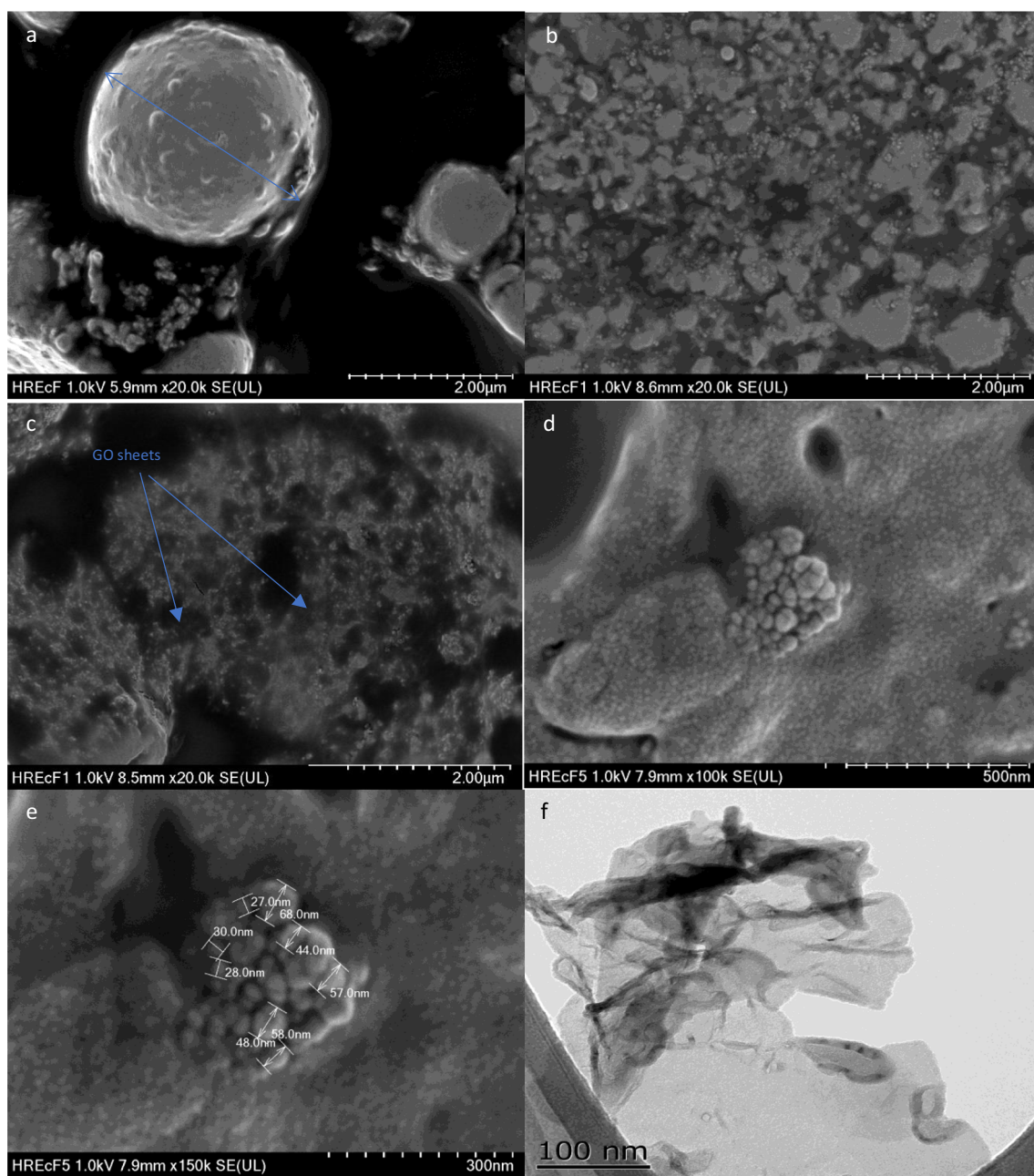
Fig. 5: SEM micrographs for (a) SiO_2 particles in the HREF, hybrid material without GO; (b) mesh of GO sheets and REF with SiO_2 on its surface for HREF1, (c) mesh of GO sheets with SiO_2 on its surface in HREF1, (d-e) agglomeration of SiO_2 particles and magnification with digital measures for HREF5 and (f) TEM micrographs of GO nanosheets alone

The follow-up with the time exposure for HREF1 is shown in Fig. 8, where the progress of the accelerated corrosion can be analyzed. Figure 8a shows the dry initial sample, Fig. 8b 170 h and Fig. 8c 340 h after the sample show no corrosion defects. After 500 h, Fig. 8d exhibits two defects. In the right upper corner and left lower corner, corrosion blistering defects appeared (2S2(2) and 2S2(2), respectively).

The test for HREF5 is displayed in Fig. 9, where the original sample can be observed in Fig. 9a. Similar to HREF1, no corrosion is observed for Fig. 9b 170 h and

Fig. 9c 340 h, however after 500 h, only one defect appeared for HREF5 as can be observed in Fig. 9d, where the right lower corner started to change its color and appearance (2S2(2)).

To complement the results, a saline immersion test was run for 600 h uninterrupted using specimens with an artificial defect completely immersed in a 5%-NaCl solution to qualitatively study the propagation of corrosion in the interphase and coating detachment in the artificial defect neighborhood.

Table 1: Adhesion, hardness, and abrasion results for specific thickness (*2 mm grid cut for thickness greater than 50 um)

Material	Thickness	Adhesion rate	Pencil scratch hardness	Abrasion max cycles
HREF	38μm	2B	4H	500
	45μm	2B	6H	2600
	52μm*	5B	7H	1600
HREF1	24μm	4B	6H	1600
	41μm	5B	7H	1200
	56μm*	5B	8H	1200
HREF5	27μm	5B	7H	1200
	49μm	5B	8H	4000
	62μm*	5B	9H	4400
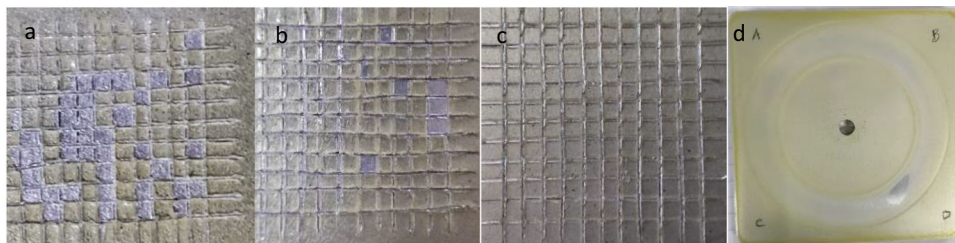
Fig. 6: Surfaces after conducting the adhesion test for (a) HREF, (b) HREF1 and (c) HREF5. (d) Specimen of HREF1 after abrasion test, where the bare metallic surface is reached

Table 2: Wear index calculations (ASTM D4060-19)

Material	HREF	HREF1	HREF5
Initial weight [g] ($\pm$ 0.05 g)	175.19	174.81	175.65
Weight after test [g] ($\pm$ 0.05 g)	175.07	174.74	175.47
Weight loss (Δg)	0.12	0.07	0.18
Mean thickness (μm)	60.4	64.4	67
Max. no of cycles	1600	1200	4000
Wear index (Δg/No. cycles)	**7.5×10^{-5}**	**6.13×10^{-5}**	**4.11×10^{-5}**

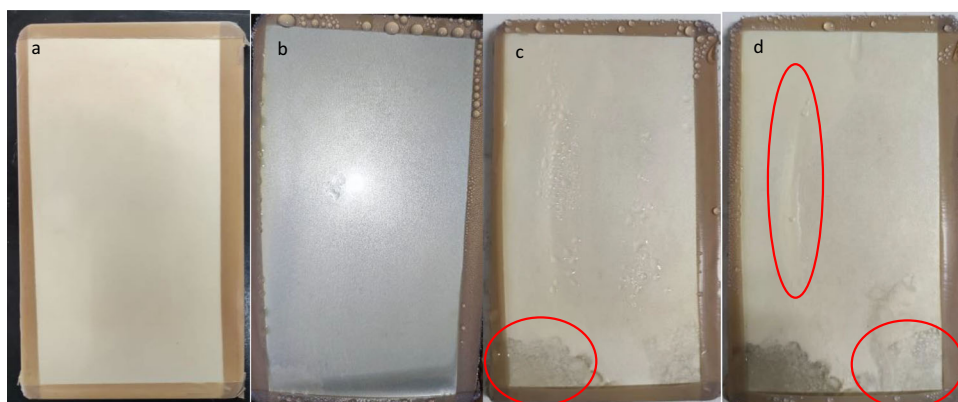In the last row for each material are shown in bold

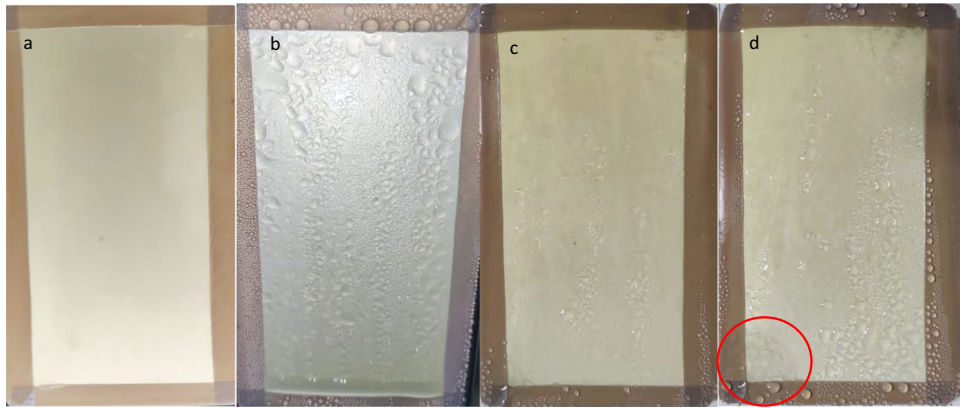**Fig. 7: Photographs of HREF in a salt fog chamber after (a) 0, (b) 170, (c) 340 and (d) 500 h**

Fig. 8: Photographs of HREF1 in a salt fog chamber after (a) 0, (b) 170, (c) 340 and (d) 500 h
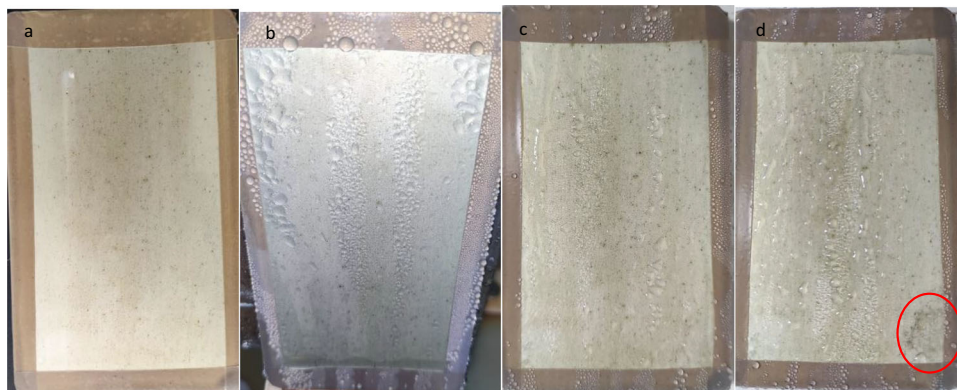

Fig. 9: Photographs of HREF5 in a salt fog chamber after (a) 0, (b) 170, (c) 340 and (d) 500 h
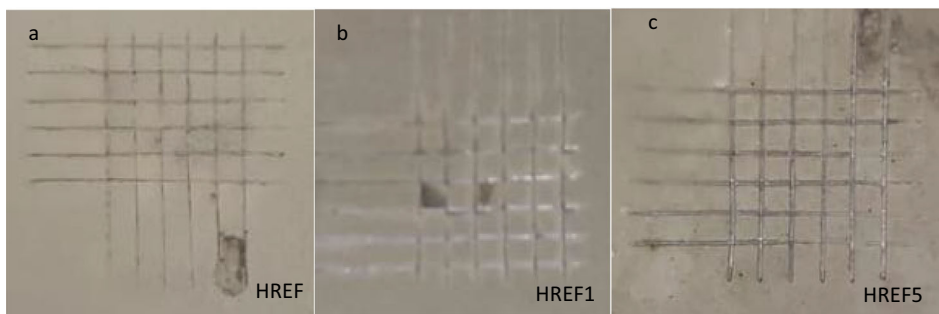

Fig. 10: Saline immersion for (a) HREF, (b) HREF1, and (c) HREF5 with artificial 2 mm grid defect. Photographs after 600 h

We can observe in Fig. 10 the final stage of the three hybrids coated in aluminum plates immersed after 600 h with artificial defects on them to study the corrosive penetration in the intersections of the defects. For HREF, only one medium-sized corrosion defect appears in the lower zone of the grid. On the other hand, HREF1 had two small corrosion defects in the interior zone of the grid and HREF5 presented one medium defect in the upper zone of the grid; however, this defect started to expand to the normal coated zone.

Electrochemical impedance spectroscopy (EIS)

This technique consists of applying a sinusoidal electric potential disturbance with a frequency variation. The impedance is calculated as the ratio between the applied potential and the current measured at the output. From the phase shift and response amplitude measurements, it is possible to obtain the electrochemical transfer impedance of the hybrid coatings studied.[34]

The Nyquist (imaginary impedance vs real impedance) plots for the hybrid materials are displayed in Fig. 11a–c. Each plot shows three curves for 0 (blue), 170 (red), and 340 h (green) within an electrochemical cell.

Figure 11a shows the EIS spectra for the HREF (0% GO). Initial impedance response was dominated by the coating capacitance and resistance for all frequencies, with a resistive component of 1.5×10^4 Ω. With increasing time (170 h), the resistance value decreased almost completely to 221.1 Ω, and a second circle appeared in the Nyquist plot where diffusion phenomena can be graphically observed at the end of the second circle. At this point, the anti-corrosive properties of HREF coating decreased considerably attributed to the major diffusion inside the coating contacting the metal interphase, causing corrosion. When the immersion time reached 340 h, the behavior was similar with the only difference being that the circles had grown due to clogged pores and aluminum passive protective layer forming. The EIS spectra of coatings HREF1 (0.1% GO) and HREF5 (0.5% GO) showed important differences compared with the HREF hybrid. As can be observed in Fig. 11b, c, the initial resistance was nearly one order of magnitude greater than the resistance of HREF coating, which indicates SiO_2/GO increased the barrier properties. After an immersion of 170 h, the resistance of the coatings was 4.5×10^4 for HREF1 and 1.4×10^5 for HREF5. A second circle started to appear in Fig. 11b, indicating that the coating had a double-layer interaction due to the coating becoming wet. Figure 11c, spectra display the best results for an immersion time of 340 h because the curve does not show a second circle, being in the first stage of degradation after that time.

In order to explain the results, a randomize numerical model was suggested to approach the curves of the spectra as equivalent electrical circuits depending on the physicochemical phenomena that occur in our studied specimen. In Fig. 12, three equivalent circuits are presented and each of them is related to the corrosion protection level. Figure 10a is the simplest equivalent circuit to which it is possible to fit the experimental data known as the Randles circuit where Rs is the solution resistance, Qc is the coating capacitance, and Rct is the coating resistance. With increasing immersion exposure time, the EIS data does not fit with the Randles circuit. Figure 12b is presented where Qdl is the capacitance of the double layer that occurs when the coating no longer provides total insulation and there are electrode/electrolyte interactions. And, Rp is the polarization resistance, and it is related to the slope of the potential-current curve in the circuit. In this second stage, the osmotic electrolyte reaches a state of saturation causing the dielectric constant to change slightly. Figure 12c represents the results of long immersion times where there is already corrosion in the working electrode and the diffusion effect is present; in the circuit it is represented with W.

In this last stage, the corrosion can be local and visible.[35]

The fitting parameters of the Nyquist plots by the EC-Lab Z-fit random-simplex method are shown in Table 3.

The wear of the coating in the presence of a corrosive electrolyte, as determined by EIS, is lower for the coatings containing GO. This characteristic is evident in the change of electrical resistance exhibited by the materials at the beginning and end of the test, calculated using an equivalent circuit approximation. For HREF5, the smallest difference in resistance (ΔRct) was obtained, with a value of 2.1×10^5 Ω, while the difference for HREF1 is 2.29×10^7 Ω (which is further increased by its high initial resistance of 2.3×10^7 Ω). Both values indicate reduced wear caused by the corrosive environment.

Regarding chemical resistance, all three coatings exhibit resistance to solvents such as acetone, hydraulic fluid, and fuel, without any visible defects. It is worth noting that none of the coatings delaminated during the rubbing process, exposing the substrate.

In the literature, the values for "Qc" capacitance for epoxy coatings are reported between the values of 1×10^{-9} and 1×10^{-11}.[35] Also, comparisons with bare and coated aluminum and steel were made for automotive research and the capacitance showed similar results between samples. The values are always in nano Faradays and the behavior, increasing or decreasing, of the species is related to the wetting capacity of the first interphase material.[36] It also allows a clue on the corrosion mechanism and its evolution over time, since this same capacitance for unprotected metal surfaces with pitting takes values around 1×10^{-4} and whether there is a protective layer depends on how compacted and porous this material is, with average values of 1×10^{-8} when pitting appears.

Bode phase diagrams are shown in Fig. 13 for further electrochemical spectra information. The Bode plot provides a graphical representation of the relationship between gain and frequency. It illustrates the magnitude of gain as a function of frequency and reveals the frequency at which the gain begins to decrease, known as the cutoff frequency. By examining the Bode plot, we can determine the stable frequency range in which the control system can operate effectively with sufficient gain. The phase and magnitude response of the loop gain in the control system indicates its stability across different frequencies of operation. It helps identify whether the system remains stable throughout the frequency range. Furthermore, it quantifies the margin available before the system becomes unstable, which can be measured in terms of phase margin and gain margin. These margins provide valuable information about the robustness of the control system and indicate how much additional phase or gain can be applied before instability occurs. The value of the impedance (Z) at low frequencies measures the corrosion resistance of the epoxy coatings, with a higher value, around a starting value of 5
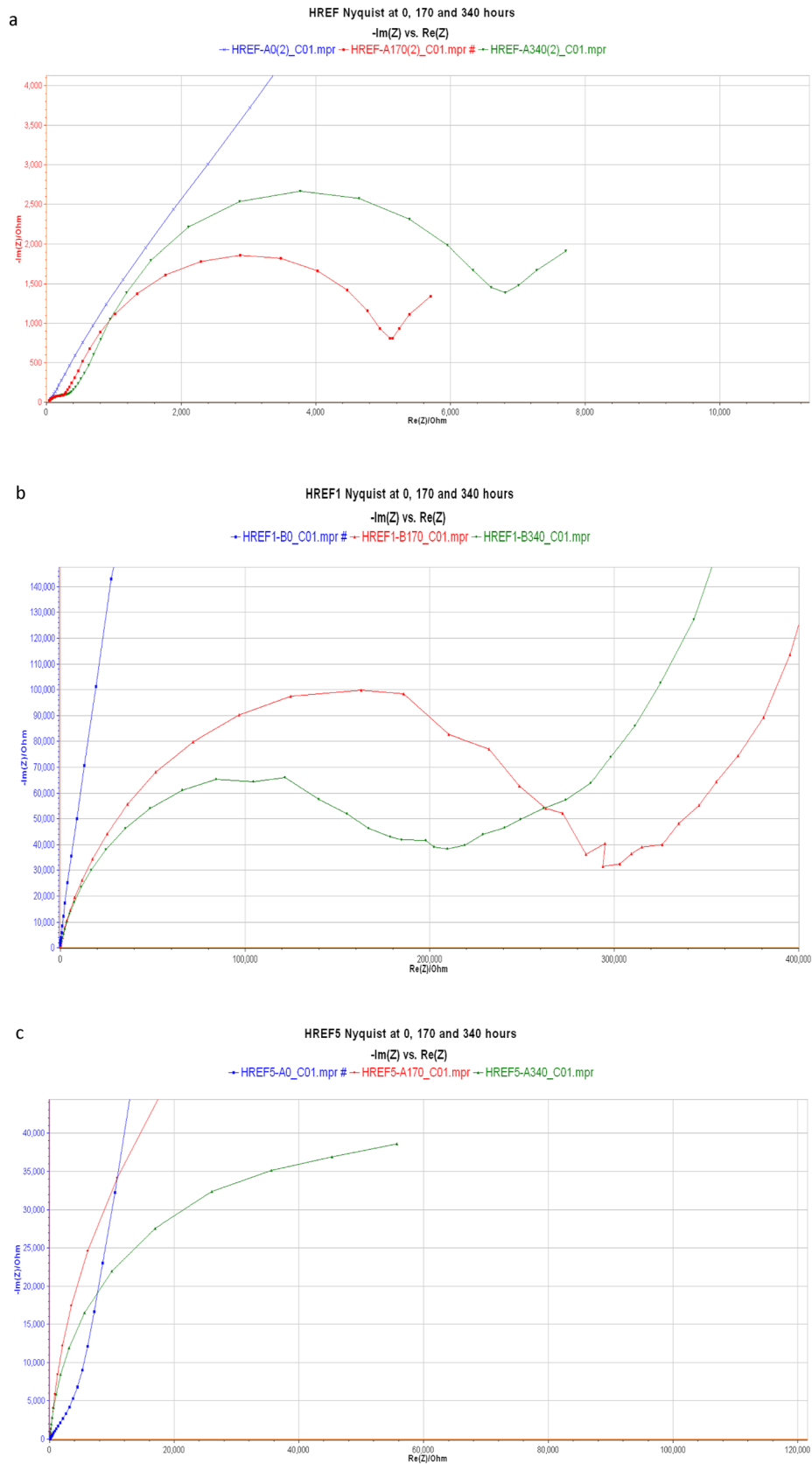
Fig. 11: Electrochemical impedance spectra Nyquist plots for (a) HREF, (b) HREF1, and (c) HREF5 at 0 (blue), 170 (red), and 340 (green) h for each material
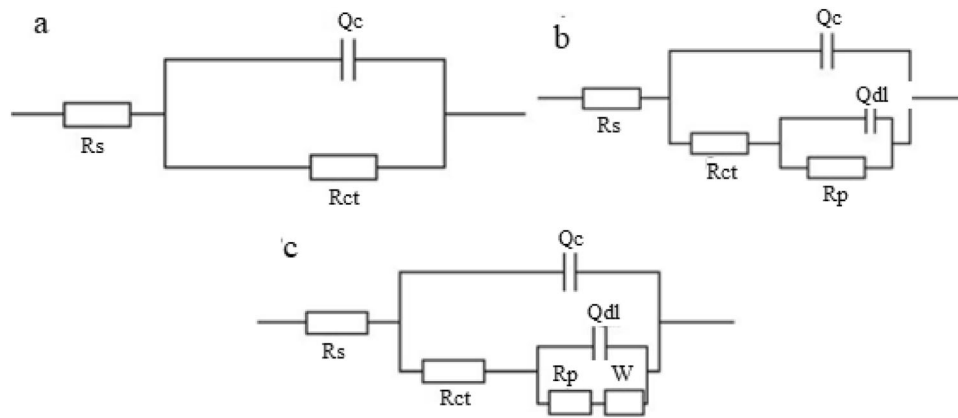
Fig. 12: Equivalent circuit models for EIS

Table 3: EIS equivalent circuit model results for each element for the hybrid coatings

Sample/time		R_s (Ω)	R_{ct} (Ω)	Q_c (F)	R_p (Ω)	Q_{dl} (F)	W ($Ω*s^{-1/2}$)
HREF (0% GO)	0 h	88.7	1.5×10^4	6.4×10^{-7}	–	–	–
	170 h	47.3	221.1	3.8×10^{-7}	4.3×10^3	40.8×10^{-6}	–
	340 h	80.9	266.5	2.7×10^{-7}	4.7×10^3	46.8×10^{-6}	659.4
HREF1 (0.1 wt% GO)	0 h	126.3	2.3×10^7	3.6×10^{-9}	–	–	–
	170 h	214.0	4.5×10^4	2.6×10^{-9}	2.1×10^5	6.1×10^{-9}	–
	340 h	227.3	3.9×10^4	2.9×10^{-9}	1.4×10^5	7.4×10^{-9}	7.1×10^4
HREF5 (0.5 wt% GO)	0 h	67.0	3.5×10^5	5.7×10^{-5}	–	–	–
	170 h	30.7	1.4×10^5	7.5×10^{-5}	–	–	–
	340 h	28.5	6.6×10^4	7.2×10^{-5}	–	–	–

on the left axis, which provides better protection on the metallic substrate.

Figure 13a–c shows that solid lines of Z value is higher for HREF1 but remains closer over time for HREF5 indicating better corrosion protection and a sign of less coating degradation or wetting.

Phase angle diagrams also evaluate the corrosion resistance. The high-frequency region indicates the degradation of the coating with the variation from negative high angle values ($-90°$) to $0°$. EIS results can be compared to other polymeric matrix coatings, including epoxy, and they fall between the operational ranges reported[37] of Z and Qc.

In the Bode diagram for HREF1 at time 0 h (Fig. 13b), there is a resonance effect inherent to the thickness and the material of the test. This behavior disappears after the coating starts to wet.

Corrosion mechanism

As observed in the previous quantitative and qualitative results, the corrosion mechanism of anti-corrosive FER-SiO$_2$/GO coatings on aluminum substrates involves the synergistic effects of graphene oxide (GO) nanosheets and silica nanoparticles. This combination provides enhanced corrosion protection by effectively blocking the flow of corrosive ions that promotes pitting and improving the chemical, thermal, and mechanical properties of the coating.

The incorporation of GO nanosheets into the epoxy matrix offers several advantages in terms of corrosion inhibition. GO has a high surface area and excellent barrier properties, which restrict the permeation of water, oxygen, and corrosive ions toward the aluminum substrate. The presence of oxygen-containing functional groups on the GO surface allows for hydrogen bonding and strong adhesion to the epoxy matrix, enhancing the coating's durability. The lamellar structure of GO nanosheets creates tortuous diffusion pathways, hindering the movement of corrosive species and providing an additional barrier against corrosion.

SiO$_2$ nanoparticles, on the other hand, contribute to the corrosion protection mechanism by providing enhanced chemical, thermal, and mechanical properties to the coating. SiO$_2$ has excellent chemical stability and acts as a protective layer, preventing the interaction of corrosive species with the aluminum substrate. It exhibits resistance to acidic and alkaline environments, reducing the degradation of the coating and ensuring long-term corrosion protection. Moreover, the high thermal stability of SiO$_2$ helps the coating
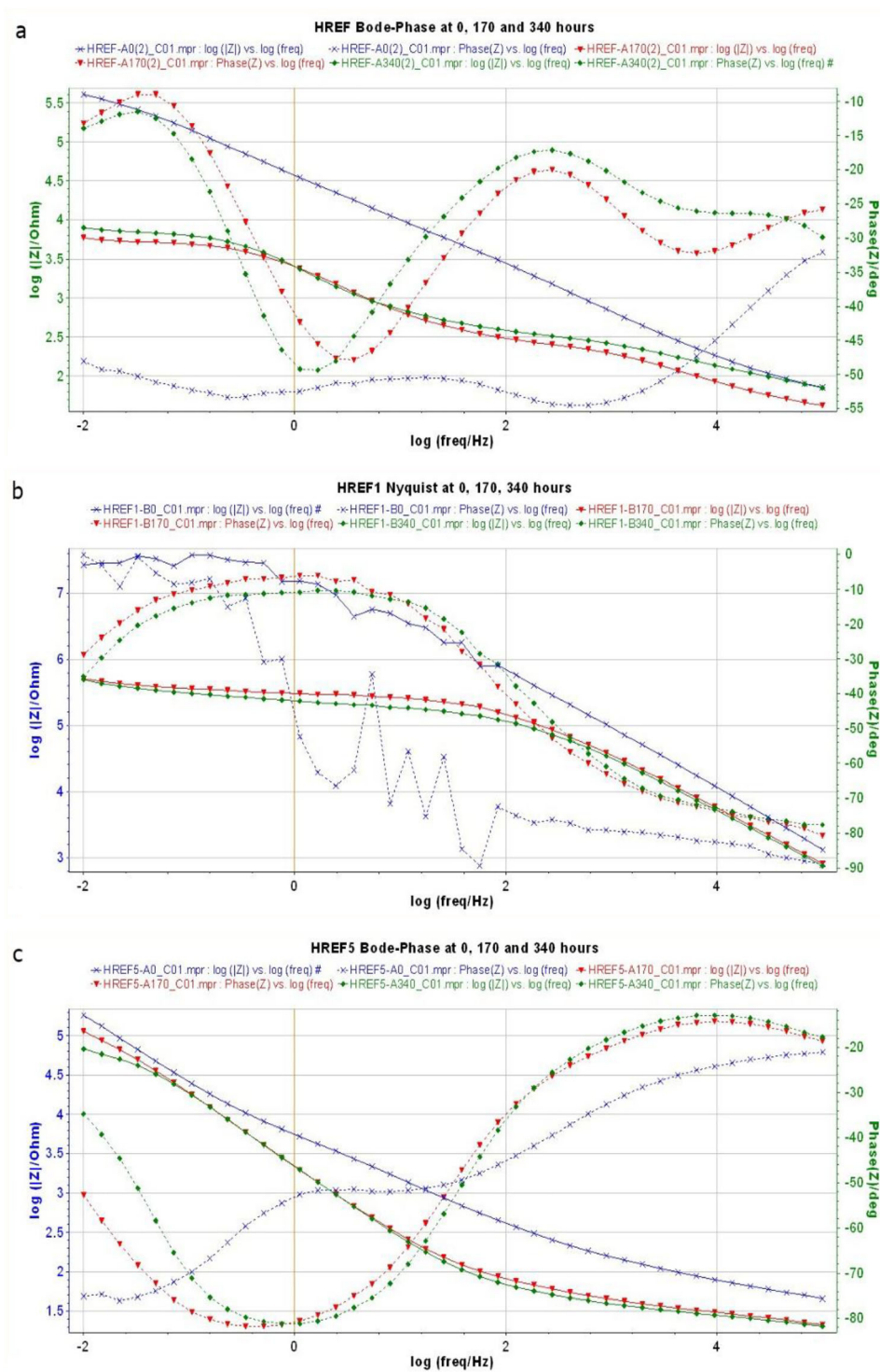
Fig. 13: Electrochemical impedance spectra Bode phase plots for HREF, HREF1, and HREF5 at 0 (blue), 170 (red), and 340 (green) h

withstand elevated temperatures without significant degradation, making it suitable for applications in harsh environments. The coating can also be further modified by incorporating other corrosion inhibitors or functional additives to provide multifunctional properties, such as self-healing capabilities or enhanced UV resistance.
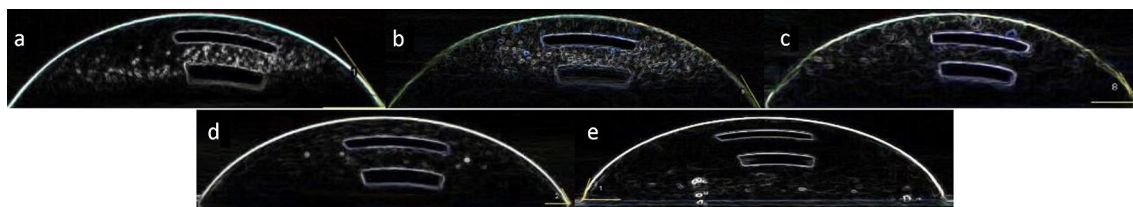
Fig. 14: Contact angle images of a water droplet on a surface with (a) neat epoxy [58.07°]; (b) abietic acid functionalized epoxy [56.15°]; (c) HREF [58.67°]; (d) HREF1 [60.23°] and (e) HREF5 [66.31°] coatings samples

Wettability

Water contact angle analysis was conducted to study the effect of SiO_2 and SiO_2/GO in the hybrid epoxy coatings systems. Three measures over eight points were selected all along the coated plate to verify the uniform distribution of all coatings. The chemical composition and surface roughness can modify the wetting ability of a coated surface. The mean values of different samples are shown in Fig. 14. The results indicated that the addition of GO increased the water contact angles from 58.07° for neat epoxy to 60.23° for HREF1 and 66.31° for HREF5. This can be attributed to the existence of bonds between the oxygen groups on the structures of GO with the SiO_2 particles enhancing the hydrophobicity. In Fig. 14, we can observe the highest contact angle value between coating species.

Conclusions

Based on the results obtained in the present work, it was clear that the introduction of SiO_2/GO in the functionalized epoxy resin to obtain hybrid materials enhanced the mechanical properties and corrosion resistance of nanofiller coating materials. The FTIR and Raman spectroscopy results corroborate the functionalization with abietic acid and the synthesis of hybrid materials identifying the carboxyl functional group. Also, there are perceptible differences when adding the graphene oxide indicating that the graphene oxide sheets are decorated with the silica particles. The morphology analysis of the materials showed that the silica particles are embedded in the polymeric matrix of the coatings with GO, HREF1 and HREF5, which is an advantage for the distribution of the SiO_2 particles, avoiding the agglomerations inside the functionalized resin matrix. This means that the SiO_2 particles are on the GO nano and microlayers decorating the basal plane.

In general, the coatings presented good resistance to accelerated corrosion, withstanding 500 h, with the HREF5-coated specimen showing the greatest resistance in the salt fog chamber test. In long-term saline immersion, the materials begin to show defects due to corrosion. Moreover, the tests for adhesion, pencil hardness and abrasion indicated that HREF5 and HREF1 had enhanced properties due to the graphene oxide concentration.

The incorporation of graphene oxide in the functionalized epoxy resin hybrid coatings presents an increment of 15% and 35% for HREF1 and HREF5, respectively, in adhesion tests. Hardness was 10% and 15% higher for HREF1 and HREF5, respectively, while the resistance to abrasion for HREF5 was considerably better with a 29.14% reduction in the wear index. The results of electrochemical impedance spectroscopy corroborate the resistance presented by the coatings after different intervals. The Rct value for HREF1 is reported to be higher, suggesting effective corrosion protection. However, taking into consideration the temporal evolution of this value it is observed that during the 0 h to 170 h stages, HREF5 demonstrates a smaller change in Rct (ΔRct) compared to HREF1. This indicates that HREF5 exhibits a more stable and consistent corrosion resistance over time, potentially making it a more suitable choice for long-term protection against corrosion.

Moreover, the wettability tests for the hybrids displayed that neither HREF nor HREF1 nor HREF5 can be considered hydrophobic materials because the contact angle for the coatings was less than 70°. However, the HREF1 and HREF5 materials do present an increase in the contact angle thanks to the incorporation of graphene oxide; this suggests a possible future work to calculate an optimal concentration or change of the hydrophobic group to obtain a better anti-freeze performance without compromising the mechanical results achieved with the incorporated GO.

Declarations

References

1. Fontana, M, *Corrosion Engineering*. McGraw-Hill Book Company, US (1985)
2. During, E, *Corrosion Atlas*. Elsevier, Netherlands (1997)
3. Zheludkevich, M, "Sol-gel Coatings for Corrosion Protection of Metals." *J. Mater. Chem.*, **15** 5099–5011 (2005)
4. Schubert, U, Husing, N, Lorenz, A, "Hybrid Inorganic-Organic Materials by Sol-Gel Processing of Organofunctional Metal Alkoxides." *Chem. Mater.*, **7** 2010–2027 (1995)
5. Araki, W, Adachi, T, "Viscoelasticity of Epoxy Resin/Silica Hybrid Material Prepared via Sol-Gel Process: Considered in Terms of Morphology." *J. Appl. Polym. Sci.*, **107** (1) 253–261 (2008)
6. Duo, S, Li, M, Zhu, M, Zhou, Y, "Resistance of Polyimide/Silica Hybrid Films to Atomic Oxygen Attack." *Surf. Coat. Technol.*, **200** 6671–6677 (2006)
7. Wen, J, Dhandapani, B, Oyama, ST, Wilkes, GL, "Preparation of Highly Porous Silica Gel from Poly(tetramethylene oxide)/Silica Hybrids." *Chem. Mater.,* **9** 1968–1971 (1997)
8. Wang, R, Zhuo, D, Zixiang, W, Wu, L, Cheng, X, Zhou, Y, Wang, J, Xuan, B, "A Novel Nanosilica/Graphene Oxide Hybrid and Its Flame Retarding Epoxy Resin with Simultaneously Improved Mechanical, Thermal Conductivity, and Dielectric Properties." *J. Mater. Chem. A*, **3** 9826–9836 (2015)
9. Zhao, X, Liu, S, Wang, X, et al. "Surface Modification of ZrO_2 Nanoparticles with a Styrene Coupling Agent and Its Effect on the Corrosion Behavior of Epoxy Coating." *Chin. J. Ocean Limnol.*, **32** 1163–1171 (2014)
10. Prasad, S, Yadav, KK, Kumar, S, Gupta, N, Cabral-Pinto, MMS, Rezania, S, Radwan, N, Alam, J, "Chromium Contamination and Effect on Environmental Health and its Remediation: A Sustainable Approaches." *J. Environ. Manag.*, **285** 112174 (2021)
11. Chu, H, Zhang, Z, Liu, Y, Leng, J, "Self-heating Fiber Reinforced Polymer Composite Using Meso/Macropore Carbon Nanotube Paper and Its Application in Deicing." *Carbon*, **66** 154–163 (2014)
12. Ramachandran, R, Kozhukhova, M, Sobolev, K, Nosonovsky, M, "Anti-icing Superhydrophobic Surfaces: Controlling Entropic Molecular Interactions to Design Novel Icephobic Concrete." *Entropy*, **18** 132–158 (2016)
13. Hejazi, V, Sobolev, K, Nosonovsky, M, "From Superhydrophobicity to Icephobicity: Forces and Interaction Analysis." *Sci. Rep.*, **3** 2194 (2013)
14. Kraj, AG, Bibeau, EL, "Phases of Icing on Wind Turbine Blades Characterized by Ice Accumulation." *Renew. Energy*, **35** 966–972 (2010)
15. Adnan, MM, Tveten, EG, Miranti, R, Hvidsten, S, Glomm Ese, M-H, Glaum, J, Einarsrud, M-A "In Situ Synthesis of Epoxy Nanocomposites with Hierarchical Surface-Modified SiO_2 Clusters." *J. Sol Gel Sci. Technol.*, **95** 783–794 (2020)
16. Devapal, D, Morris, VB, Suraj, S, Packirisamy, S, "Nonaqueous Sol–Gel Synthesis of Epoxy-Functionalized and Epoxy and Vinyl-functionalized Poly(borosiloxane)s." *J. Sol-Gel Sci. Technol.*, **107** 133–148 (2023)
17. Zheng, H, Shao, Y, Wang, Y, et al. "Reinforcing the Corrosion Protection Property of Epoxy Coating by Using Graphene Oxide-Poly(urea-formaldehyde) Composites." *Corros. Sci.*, **123** 267–277 (2017)
18. Parhizkar, N, Sharabi, T, Ramezanzadeh, B, "A New Approach for Enhancement of the Corrosion Protection Properties and Interfacial Adhesion Bonds Between the Epoxy Coating and Steel Substrate Through Surface Treatment by Covalently Modified Amino Functionalized Graphene Oxide Film." *Corros. Sci.*, **123** 55–75 (2017)
19. Pourhashem, S, Vaezi, M, Rashudu, A, "Exploring Corrosion Protection Properties of Solvent Based Epoxy-Graphene Oxide Nanocomposite Coatings on Mild Steel." *Corros. Sci.*, **115** 78–92 (2017)
20. Najafi-Shoa, S, Roghani-Mamaqani, H, Salami-Kalajahi, M, "Incorporation of Epoxy Resin and Graphene Nanolayers into Silica Xerogel Network: An Insight into Thermal Improvement of Resin." *J. Sol-Gel Sci. Technol.*, **80** 362–377 (2016)
21. Haeri, Z, Ramezanzadeh, B, Asghari, M, "A Novel Fabrication of a High Performance SiO_2 Graphene Oxide (GO) Nanohybrids: Characterization of Thermal Properties of Epoxy Nanocomposites Filled with SiO_2-GO Nanohybrids." *J. Colloid Interface Sci.*, **493** 111–122 (2017)
22. Ramezanzadeh, B, Haeri, H, Ramezanzadeh, M, "A Facile Route of Making Silica Nanoparticles-Covered Graphene Oxide Nanohybrids (SiO_2-GO); Fabrication of SiO_2-GO/epoxy Composite Coating with Superior Barrier and Corrosion Protection Performance." *Chem. Eng. J.*, **303** 511–528 (2016)
23. Ramezanzadeh, B, Niroumandrad, S, Ahmadi, A, et al. "Enhancement of Barrier and Corrosion Protection Performance of an Epoxy Coating Through Wet Transfer of Amino Functionalized Graphene Oxide." *Corros. Sci.*, **103** 283–304 (2016)

24. Hummers, Jr, WS, Offeman, RE, "Preparation of Graphitic Oxide." *J. Am. Chem. Soc.,* **80** 1339–1339 (1958)

25. Hernández-Padrón, G, García-Garduño, M, "Sol-gel, One Technology by Produced Nanohybrid with Anticorrosive Properties." *Phys. Procedia,* **48** 102–108 (2013)

26. Ramirez-Palma, MT, Hernández-Padron, G, Mójica-Gómez, J, Rojas-Gonzales, F, Castaño, VM, "Nanostructured Epoxy-Based Anticorrosive Coatings." *Surface Rev. Lett.,* **27** 9 (2020)

27. *ASTM D-2369-20 Standard Test Method for Volatile Content of Coatings*

28. *ASTM D3363-20 Standard Test Method for Film Hardness by Pencil Test*

29. *ASTM D4060-19; Standard Test Method for Abrasion Resistance of Organic Coatings by Taber Abraser*

30. *ASTM D3359-17 Standard Test Methods for Rating Adhesion by Tape Test*

31. Drewniak, S, Muzyka, R, Stolarczyk, A, Pustelny, T, Setkiewicz, M, "Studies of Reduced Graphene Oxide and Graphite Oxide in the Aspect of Their Possible Application in Gas Sensors." *Sens. MDPI,* **16** 103 (2016)

32. Chen, P-H, Sie, M-C, Jeng, P-D, Wu, R-C, Wang, C-B, "Graphene Sponge as an Efficient and Recyclable Oil Sorbent." *AIP Conference Proceedings,* no. **1877** (2017)

33. Hernández-Padrón, G, García-Garduño, M, Rojas-González, F, "Hybrid Materials Based on Functionalized Epoxy Resin Networks." *Pigment Resin Technol.,* **39** (4) 195–202 (2010)

34. Aghiles, B, Rachida, D, "Synthesis and Characterization of Hybrid Materials Based on Graphene Oxide and Silica Nanoparticles and Their Effect on the Corrosion Protection Properties of Epoxy Resin Coatings." *J. Adhes. Sci. Technol.,* **33** (8) 834–860 (2019)

35. Wang, N, Gao, H, Zhang, J, Kang, P, "Effect of Graphene Oxide/ZSM-5 Hybrid on Corrosion Resistance of Waterborne Epoxy Coating." *Coatings,* **8** (179) 14 (2018)

36. Suay, J, Rodríguez, M, Razzaq, K, Carpio, J, Saura, J, "The Evaluation of Anticorrosive Automotive Epoxy Coatings by Means of Electrochemical Impedance Spectroscopy." *Prog. Org. Coat.,* **46** 121–129 (2003)

37. Zheng, SX, Li, JH, "Inorganic–Organic Sol Gel Hybrid Coatings for Corrosion Protection of Metals." *J. Sol-Gel Sci. Technol.,* **54** 174–187 (2010)